Frontiers of Information Technology & Electronic Engineering
www.jzus.zju.edu.cn; engineering.cae.cn; www.springerlink.com
ISSN 2095-9184 (print); ISSN 2095-9230 (online)
E-mail: jzus@zju.edu.cn

Zirconia quantum dots for a nonvolatile resistive random access memory device*

Xiang-lei HE[1], Rui-jie TANG[1], Feng YANG[†‡2], Mayameen S. KADHIM[2], Jie-xin WANG[1], Yuan PU[1], Dan WANG[†‡1]

[1]*State Key Laboratory of Organic-Inorganic Composites, Beijing University of Chemical Technology, Beijing 100029, China*

[2]*MOE Key Laboratory of Advanced Technology of Materials, School of Materials Science and Engineering, Southwest Jiaotong University, Chengdu 610031, China*

[†]E-mail: yf@swjtu.edu.cn; wangdan@mail.buct.edu.cn

Received July 19, 2019; Revision accepted Nov. 14, 2019; Crosschecked Dec. 12, 2019

Abstract: We propose a nonvolatile resistive random access memory device by employing nanodispersion of zirconia (ZrO_2) quantum dots (QDs) for the formation of an active layer. The memory devices comprising a typical sandwich structure of Ag (top)/ZrO_2 (active layer)/Ti (bottom) are fabricated using a facile spin-coating method. The optimized device exhibits a high resistance state/low resistance state resistance difference (about 10 Ω), a good cycle performance (the number of cycles larger than 100), and a relatively low conversion current (about 1 μA). Atomic force microscopy and scanning electron microscope are used to observe the surface morphology and stacking state of the ZrO_2 active layer. Experimental results show that the ZrO_2 active layer is stacked compactly and has a low roughness (Ra=4.49 nm) due to the uniform distribution of the ZrO_2 QDs. The conductive mechanism of the Ag/ZrO_2/Ti device is analyzed and studied, and the conductive filaments of Ag ions and oxygen vacancies are focused on to clarify the resistive switching memory behavior. This study offers a facile approach of memristors for future electronic applications.

Key words: Zirconia quantum dot; Resistive switching; Memory device; Spin coating
https://doi.org/10.1631/FITEE.1900363 **CLC number:** TN386.1

1 Introduction

In the information age, given the continuous developments of computer technology and the universal applications of smartphones, the means of storing information is particularly important (Han et al., 2017, 2018; Jiang et al., 2017; Craig, 2018; Wan et al., 2018; Vescio et al., 2019). However, in the architecture adopted in traditional computers, computing and storaging functions are separated and performed by a central processing unit (CPU) and the memory, respectively (Liu et al., 2017; Zhou et al., 2018; Wang et al., 2019). While the speed and capacity of the CPUs and memory are increasing rapidly, increases of bus speed for transferring data and instructions have been quite limited. Memristors or resistance random access memory (RRAM) can be used to not only store data but also implement logic calculations (Pan et al., 2014). Therefore, RRAM can effectively solve the problem of the speed mismatch between a CPU and memory, and improve information processing efficiency. Strukov et al. (2008) proved the existence of resistive switching memory through a physical experiment, which initiated an upsurge in the RRAM research. Memristors have demonstrated that they can realize high resistance

‡ Corresponding authors
* Project supported by the National Natural Science Foundation of China (No. 21808009) and the Beijing Natural Science Foundation, China (No. 2182051)
ORCID: Xiang-lei HE, http://orcid.org/0000-0003-4995-0085; Feng YANG, http://orcid.org/0000-0003-2028-5704; Dan WANG, http://orcid.org/0000-0002-3515-4590
© Zhejiang University and Springer-Verlag GmbH Germany, part of Springer Nature 2019

state (HRS) ("Off" state) and low resistance state (LRS) ("On" state) conversion during operation. If the HRS or "Off" state in the logic is regarded as "0," the LRS or "On" state in the logic is regarded as "1," then the RRAM can realize information storage in a binary form (Sun et al., 2018b). Therefore, in recent years, memristors have been considered the most promising candidates for the new generation of non-volatile storage devices (Chua, 2011; Kadhim et al., 2018).

Memristors can be prepared from a wide variety of sources, such as metal oxides (Liang et al., 2015; Lyu et al., 2015; Sun et al., 2018a; Yu et al., 2018), perovskites (Yan et al., 2016; Zhang et al., 2017), two-dimensional layered materials (Han et al., 2017; Zhao et al., 2017), and biological material (Sun et al., 2018b). Metal-oxide structures have been extensively studied due to their low cost and simple preparation process, and zirconia (ZrO_2) has emerged as a prospective candidate for the active functional layer in memory devices (Emelyanov et al., 2019). ZrO_2 has many advantages, such as a high dielectric constant, stable chemical properties, nontoxicity, and simple composition (Panda and Tseng, 2013; Xia et al., 2018). Therefore, ZrO_2 has been widely applied to the preparation of a variety of optical and electronic devices (Panda and Tseng, 2013; He et al., 2019a). Recently, due to the various advantages of ZrO_2, RRAM devices based on a ZrO_2 active layer have been proposed (Emelyanov et al., 2019). However, the preparation methods for RRAM devices are complex, as they usually involve a magnetron sputtering method (Wang et al., 2011; Emelyanov et al., 2019). As far as we know, using a simple spin-coating method for the preparation of an Ag/ZrO_2/Ti sandwich structure has rarely been reported. In this work, aqueous nanodispersion of ZrO_2 quantum dots (QDs), prepared using a hydrothermal method coupled with alkaline hydrogen peroxide (AHP) process, is used for the formation of an active layer in the memristor of the memory devices fabricated in a typical Ag/ZrO_2/Ti sandwich structure. The optimized device shows an HRS/LRS resistance difference (about 10 Ω), a good cycle performance (the number of cycles larger than 100), and a relatively low conversion current (about 1 μA) at room temperature. In this work, we demonstrate the potential applications of ZrO_2 QDs as an active layer in the fabrication of high-performance memory devices through a simple spin-coating method.

2 Experiments

2.1 Preparation of aqueous nanodispersion of ZrO_2 QDs

Aqueous nanodispersion of ZrO_2 QDs was synthesized using a conventional hydrothermal method coupled with an AHP process (He et al., 2019b). Zirconium carbonate basic (ZCB, CAS:57219-64-4, ZrO_2 content>40%), sodium hydroxide (NaOH, 99.99%), hydrogen peroxide (H_2O_2, 30%), and nitric acid as sources for reactions were purchased from the Aladdin Co., Ltd. (Shanghai of China), to prepare the aqueous ZrO_2 nanodispersion. Deionized water was depurated using a Smart-S30 water purification system (Hitech). For a typical experiment, 20 g NaOH, 20 g ZCB, and 40 g deionized water were weighed and heated in a hydrothermal kettle at 110 °C for 6 h. All the products (including solids and liquids) were moved from the hydrothermal kettle to a 250-mL round bottom flask, and then 85 mL deionized water was added to dilute them. Finally, 5.1 mL H_2O_2 was added at 50 °C for 5 h under vigorous stirring. Subsequently, the excess alkali solution was removed using a decantation process and the wet solids were washed repeatedly with deionized water to remove the excess ions. Finally, the wet solids were added to a diluted nitric acid solution (1.5 mol/L) to turn them into transparent and stable aqueous ZrO_2 nanodispersion after stirring.

2.2 Preparation of Ag/ZrO_2/Ti sandwich structural memristors

Fig. 1 shows the manufacturing process of the Ag/ZrO_2/Ti sandwich structure. First, titanium foils (1 cm×3 cm×0.1 mm) were cleaned with alcohol in an ultrasound bath. Then, the titanium foil was fixed on a spin coater (KW-4A), and aqueous nanodispersion of ZrO_2 QDs with a 1% solid content was pipetted onto the titanium foil with a pipette. The spin coater was set to 5 s (500 r/min) for the first cycle and 20 s (1500 r/min) for the second cycle. The titanium foil loaded with the ZrO_2 nanoparticle layer was then

dried in a vacuum oven at 90 °C for 6 h. Then, Ag was sputtered on the top of the ZrO_2 QD layer using a metal shadow mask to form the sandwich structure.

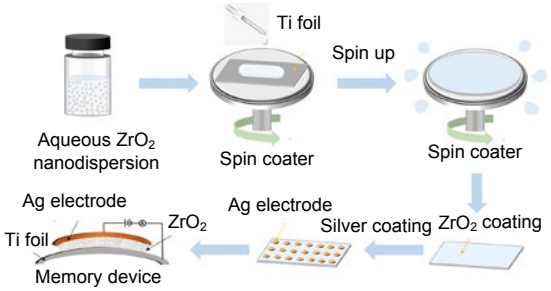

Fig. 1 Manufacturing process of the Ag/ZrO_2/Ti device

2.3 Characterization

The hydrated particle size of the ZrO_2 QDs in the aqueous solution was tested by dynamic light scattering (DLS, Malvern Nano ZS90, England). The density of the stacked layers and coating morphology of the ZrO_2/Ti foil were examined using scanning electron microscope (SEM, Hitachi S4800). The surface morphology of the ZrO_2/Ti foil was also investigated by atomic force microscopy (AFM, Bruker Dimension Icon, Germany) with tapping-mode pattern. The magnitude and morphology of the ZrO_2 nanoparticles were obtained using transmission electron microscope (TEM, Hitachi HT-7700). The lattice structure and size of the ZrO_2 QDs were determined by high-resolution TEM (HRTEM, Hitachi H-9500). The particle size of the ZrO_2 QDs in the TEM was statistically analyzed using the Nano Measurer software. The X-ray diffraction (XRD) patterns of the samples were measured using an XRD-6000 diffractometer (Shimadzu Inc.). The current-voltage (*I*-*V*) curves of the Ag/ZrO_2/Ti devices were measured with a CHI 660B electrochemical workstation (CH Instruments).

3 Results and discussion

ZrO_2 QDs prepared using the hydrothermal method and AHP treatment are characterized (Fig. 2). According to the DLS results (Fig. 2a), the *z*-average particle diameter of the aqueous ZrO_2 nanodispersion was 14.52 nm and the PDI value was 0.370, showing that the AHP-treated ZrO_2 QDs had good

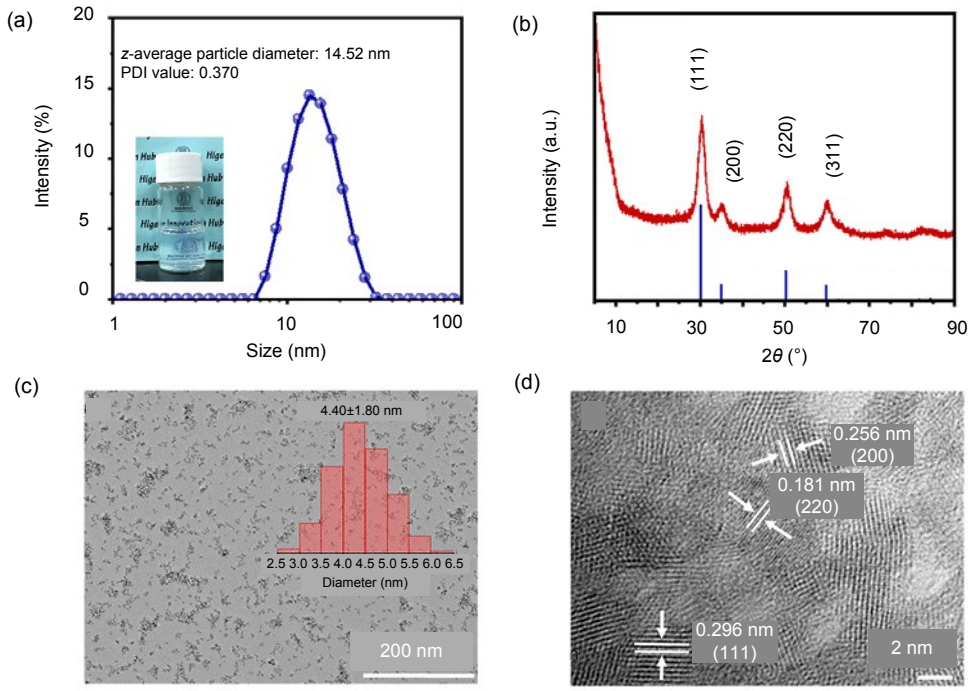

Fig. 2 Characterization of ZrO_2 QDs: (a) DLS results of aqueous ZrO_2 nanodispersion (inset: ZrO_2 nanodispersion with 1% solid content); (b) XRD curve of the ZrO_2 nanopowder; (c) morphologies and structural characteristic of aqueous ZrO_2 nanodispersion (inset: particle size distributions of single ZrO_2 particles); (d) HRTEM of ZrO_2 QDs

dispersibility in water. Fig. 2b shows that the phase of hydrophilic ZrO_2 QDs was the single cubic phase (JCPDS: 49-1642) given their XRD patterns. The diffraction peaks were observed at 30.12°, 34.96°, 50.22°, and 59.74°, corresponding to the crystal planes of (111), (200), (220), and (311), respectively. The ZrO_2 QDs with cubic phase had the highest density and the most stable structure in the three crystal phases of ZrO_2, and were an ideal choice for optoelectronic applications (He et al., 2019b). Fig. 2c shows a TEM image of the aqueous ZrO_2 nanodispersion, which had an average particle size of 4.40 nm. It can be seen from the TEM image that the ZrO_2 QDs did not reach a monodisperse state, but mainly a small agglomeration formed by several particles. This corresponds to the DLS results that a small agglomeration formed mainly by 2–5 ZrO_2 QDs was obtained. Using the inorganic zirconium source as a raw material to prepare the ZrO_2 QDs, the growth of the hydroxyl group on the surface of the ZrO_2 was promoted only by the oxidation of H_2O_2. It is not easy to obtain such a grade of aqueous ZrO_2 nanodispersion without adding other surfactants or modifiers. At the same time, the surface of the ZrO_2 QDs was treated by H_2O_2, which can increase the number of defect sites. The proportion of defect sites in the layer is related to the performance of the memristors. However, in this preparation method, factors such as surfactants or modifiers that can influence the performance of the memristors are avoided. In Fig. 2d, different lattice lengths can be observed to determine different crystal planes, in which (111) corresponds to 0.296 nm, (220) corresponds to 0.181 nm, and (200) corresponds to 0.256 nm. This corresponds to the XRD results, demonstrating that the crystal phase of ZrO_2 QDs was the cubic phase.

Figs. 3a and 3b show the surface structure of the ZrO_2-coated titanium foil. The hydrophilic ZrO_2 coating clearly showed a film formed by stacking a dense oxide on the titanium sheet. The thickness of the ZrO_2 coating was observed by SEM at around 500 nm (Fig. 3c). Fig. 3d depicts a three-dimensional AFM image of the ZrO_2 coating on the titanium foil. The average surface roughness (Ra) of the ZrO_2 surface coating was 4.49 nm, which was close to the size of a single ZrO_2 QD.

Fig. 4a shows the consecutive *I-V* curves of the Ag/ZrO_2/Ti sandwich structure, which was examined at a scanning rate of 0.1 V/ms from 0→1.5→0→−1.5→0 V. To avoid permanent electrical breakdown of the Ag/ZrO_2/Ti device, the compliance current was secured at 0.5 A. Results show that the device had a quick response even in very short time and a relatively low switching current (about 1 μA). At the same time, it is found that the device exhibited a very typical resistive switching performance. As the forward voltage decreased backswept, the device transferred from LRS to HRS. Fig. 4b shows a resistive switching behavior in a single cyclic sweep, which exhibited good "Set" and "Reset" performances. Considering the practical application of memristors, a stable cycle performance and a large HRS/LRS resistance difference are necessary.

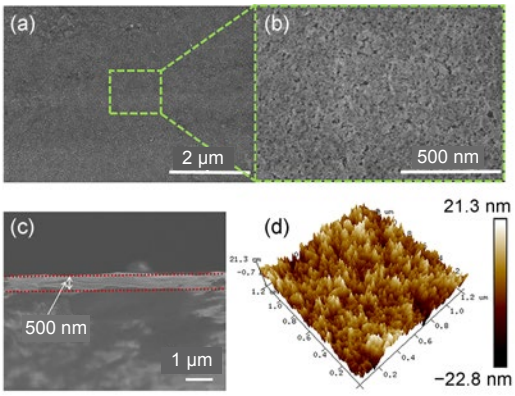

Fig. 3 SEM images (a and b), the cross sectional SEM image (c), and an AFM image (d) of ZrO_2 coating on the titanium foil

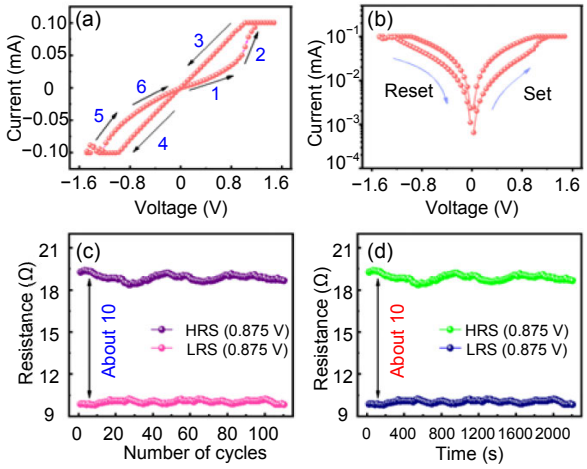

Fig. 4 *I-V* curves of a single cycle when the voltage changes from 0→1.5→0→−1.5→0 V (a and b), and resistance curves vs. the number of cycles and time under a positive voltage of 0.875 V (c and d)

The resistance difference was obtained by contrasting the current density of the LRS ("On" state) with that of the HRS ("Off" state) at a specific voltage (0.875 V). Resistance memories of both the HRS and LRS were calculated (Figs. 4c and 4d). Results show that the HRS/LRS resistance difference was about 10 Ω. It is also shown that the HRS/LRS resistance difference remained constant under a long cycle (the number of cycles larger than 100). The above results show that the Ag/ZrO_2/Ti device has a stable performance.

To realize the resistive switching mechanism in the devices, the curve was secured at a log-log scale (Figs. 5a and 5b). Figs. 5a and 5b show the *I-V* curves in the negative and positive voltage sections of the Ag/ZrO_2/Ti device, respectively. Fig. 5a represents the charges distributed through the Ag anode into the ZrO_2 active layer, leading to the conduction mechanism (Sleiman et al., 2012). The slope of this partial linear portion was 1.036 (close to 1), indicating Ohmic conductance. As the applied voltage increased, the log *I* vs. log *V* had a linear correlationship and the slope was 2.29 (Fig. 5a), indicating $I \propto V^m$. Therefore, the conduction performance of the Ag/ZrO_2/Ti device followed the regulation of classical trap-controlled space charge limited conduction (SCLC) (Siddiqui et al., 2017). It shows that the charge transfer happened between the Ag electrode and the ZrO_2 layer. This can be demonstrated by the formation of the Ag conductive filaments (Kadhim et al., 2018).

In the LRS of the positive part, the *I-V* curve was well secured through the Ohmic conductance performance with a slope of about 0.99. SCLC in semiconductors and their corresponding space charge effects were important basic concepts. The SCLC model generally contains three regimes: low voltage Ohmic region ($I \propto V$), Child's square region ($I \propto V^2$), and current steep increase region ($I \propto V^m$, $m>2$). The formula for the SCLC model is expressed as follows (Vishwanath and Kim, 2016):

$$J \propto V^{m+1} / t^{2m+1}, \tag{1}$$

where *J*, *V*, *t*, and *m* are the current density of ZrO_2, bias voltage, thickness, and fitting index, respectively. When m=0, Eq. (1) represents the Ohmic conductance behavior. If m=1, it becomes a Child's square law, which is given by (Vishwanath and Kim, 2016; Li et al., 2017)

$$J \propto \frac{9}{8} \varepsilon_0 \varepsilon_r \mu \frac{V^2}{t^3}, \tag{2}$$

where μ, ε_0, and ε_r are the carrier mobility, vacuum dielectric constant, and relative dielectric constant, respectively. In this work, Ag atoms in the Ag electrode of the Ag/ZrO_2/Ti devices were ionized into Ag ions by the application of an electric field. This behavior can be described as $Ag^+ + e^- \rightarrow Ag$ (Sun et al., 2014; Zhou et al., 2017).

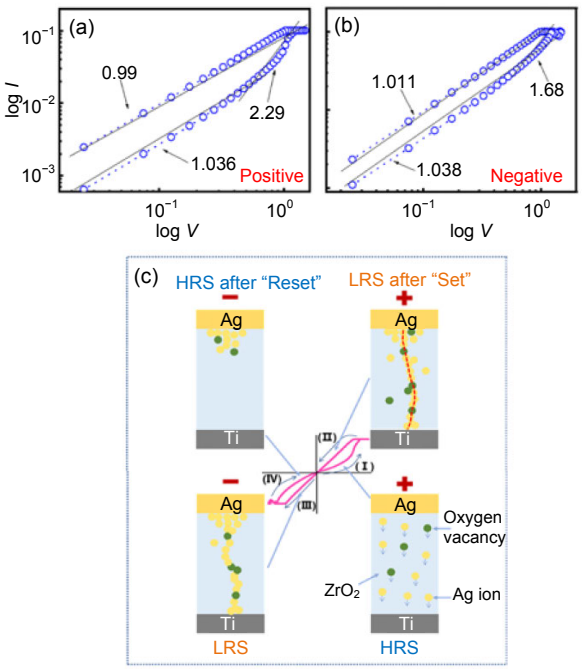

Fig. 5 *I-V* curves of the Ag/ZrO_2/Ti structure device (a and b) and the speculative model of Ag ion and oxygen vacancy filaments (c)

At the same time, the possible formation of conductive filaments was analyzed. The Ag ions can move along the electric field direction in the applied electric field (Fig. 5c). When the Ag ions and oxygen vacancies accumulated to a certain extent, the conductivity of the ZrO_2 active layer was greatly increased, because the Ag ions and oxygen vacancies acted as conductive filaments, and this process corresponded to the "Set" process of resistance switching (Wu et al., 2017). After the "Set" process, the device retained the LRS ("On" state) until a large voltage of opposite polarity ($<V_{Reset}$) dissolved the Ag and

oxygen vacancy filaments, with this route corresponding to "Reset" of the Ag/ZrO_2/Ti device, following which the Ag ions and oxygen vacancies were moved back to the Ag electrode. Therefore, the Ag/ZrO_2/Ti device can be reversibly switched by connecting and disconnecting conducting filaments.

4 Conclusions

In this work, nonvolatile resistive random access memory devices using ZrO_2 QDs as an active layer have been devised via a simple spin-coating process. The resistive switching memory devices based on Ag (top)/ZrO_2 (active layer)/Ti (bottom) showed an HRS/LRS resistance difference (about 10 Ω), a good cycle performance (the number of cycles larger than 100), and a relatively low conversion current (about 1 μA). This result revealed that the Ag ions and oxygen vacancies are organized as conducting filaments inside the ZrO_2 coating, and provided a new approach to nonvolatile memory devices based on a ZrO_2 active layer for further electronic applications.

Compliance with ethics guidelines

Xiang-lei HE, Rui-jie TANG, Feng YANG, Mayameen S. KADHIM, Jie-xin WANG, Yuan PU, and Dan WANG declare that they have no conflict of interest.

References

Chua L, 2011. Resistance switching memories are memristors. *Appl Phys A*, 102(4):765-783. https://doi.org/10.1007/s00339-011-6264-9

Craig J, 2018. Cybersecurity research—essential to a successful digital future. *Engineering*, 4(1):9-10. https://doi.org/10.1016/j.eng.2018.02.006

Emelyanov AV, Nikiruy KE, Demin VA, et al., 2019. Yttria-stabilized zirconia cross-point memristive devices for neuromorphic applications. *Microelectron Eng*, 215: 110988. https://doi.org/10.1016/j.mee.2019.110988

Han PD, Sun B, Li J, et al., 2017. Ag filament induced non-volatile resistive switching memory behaviour in hexagonal $MoSe_2$ nanosheets. *J Coll Interf Sci*, 505:148-153. https://doi.org/10.1016/j.jcis.2017.05.082

Han WB, Chen XG, Li SF, et al., 2018. A novel non-volatile memory storage system for I/O-intensive applications. *Front Inform Technol Electron Eng*, 19(10):1291-1302. https://doi.org/10.1631/FITEE.1700061

He XL, Tang RG, Pu Y, et al., 2019a. High-gravity-hydrolysis approach to transparent nanozirconia/silicone encapsulation materials of light emitting diodes devices for healthy lighting. *Nano Energy*, 62:1-10. https://doi.org/10.1016/j.nanoen.2019.05.024

He XL, Wang Z, Wang D, et al., 2019b. Sub-kilogram-scale synthesis of highly dispersible zirconia nanoparticles for hybrid optical resins. *Appl Surf Sci*, 491:505-516. https://doi.org/10.1016/j.apsusc.2019.06.187

Jiang H, Belkin D, Savel′ev SE, et al., 2017. A novel true random number generator based on a stochastic diffusive memristor. *Nat Commun*, 8(1):882. https://doi.org/10.1038/s41467-017-00869-x

Kadhim MS, Yang F, Sun B, et al., 2018. A resistive switching memory device with a negative differential resistance at room temperature. *Appl Phys Lett*, 113(5):053502. https://doi.org/10.1063/1.5037191

Li XM, Tao L, Chen ZF, et al., 2017. Graphene and related two-dimensional materials: structure-property relationships for electronics and optoelectronics. *Appl Phys Rev*, 4(2):021306. https://doi.org/10.1063/1.4983646

Liang L, Li K, Xiao C, et al., 2015. Vacancy associates-rich ultrathin nanosheets for high performance and flexible nonvolatile memory device. *J Am Chem Soc*, 137(8): 3102-3108. https://doi.org/10.1021/jacs.5b00021

Liu X, Lu YT, Yu J, et al., 2017. ONFS: a hierarchical hybrid file system based on memory, SSD, and HDD for high performance computers. *Front Inform Technol Electron Eng*, 18(12):1940-1971. https://doi.org/10.1631/FITEE.1700626

Lyu MJ, Liu YW, Zhi YD, et al., 2015. Electric-field-driven dual vacancies evolution in ultrathin nanosheets realizing reversible semiconductor to half-metal transition. *J Am Chem Soc*, 137(47):15043-15048. https://doi.org/10.1021/jacs.5b10212

Pan F, Gao S, Chen C, et al., 2014. Recent progress in resistive random access memories: materials, switching mechanisms, and performance. *Mater Sci Eng R Rep*, 83:1-59. https://doi.org/10.1016/j.mser.2014.06.002

Panda D, Tseng TY, 2013. Growth, dielectric properties, and memory device applications of ZrO_2 thin films. *Thin Sol Film*, 531:1-20. https://doi.org/10.1016/j.tsf.2013.01.004

Siddiqui GU, Rehman MM, Choi KH, 2017. Resistive switching phenomena induced by the heterostructure composite of $ZnSnO_3$ nanocubes interspersed ZnO nanowires. *J Mater Chem C*, 5(22):5528-5537. https://doi.org/10.1039/c7tc01105a

Sleiman A, Mabrook MF, Nejm RR, et al., 2012. Organic bistable devices utilizing carbon nanotubes embedded in poly (methyl methacrylate). *J Appl Phys*, 112(2):024509. https://doi.org/10.1063/1.4737599

Strukov DB, Snider GS, Stewart DR, et al., 2008. The missing memristor found. *Nature*, 453(7191):80-83. https://doi.org/10.1038/nature06932

Sun B, Li HW, Wei LJ, et al., 2014. Hydrothermal synthesis and resistive switching behaviour of $WO_3/CoWO_4$ core-shell nanowires. *Cryst Eng Comm*, 16(42):9891-9895. https://doi.org/10.1039/C4CE01442A

Sun B, Zhu SH, Mao SS, et al., 2018a. From dead leaves to sustainable organic resistive switching memory. *J Coll Interf Sci*, 513:774-778. https://doi.org/10.1016/j.jcis.2017.12.007

Sun B, Zhang XJ, Zhou GD, et al., 2018b. A flexible non-volatile resistive switching memory device based on ZnO film fabricated on a foldable PET substrate. *J Coll Interf Sci*, 520:19-24. https://doi.org/10.1016/j.jcis.2018.03.001

Vescio G, Martín G, Crespo-Yepes A, et al., 2019. Low-power, high-performance, non-volatile inkjet-printed HfO_2-based resistive random access memory: from device to nanoscale characterization. *ACS Appl Mater Interf*, 11(26):23659-23666. https://doi.org/10.1021/acsami.9b01731

Vishwanath SK, Kim J, 2016. Resistive switching characteristics of all-solution-based Ag/TiO_2/Mo-doped In_2O_3 devices for non-volatile memory applications. *J Mater Chem C*, 4(46):10967-10972. https://doi.org/10.1039/c6tc03607d

Wan T, Qu B, Du HW, et al., 2018. Digital to analog resistive switching transition induced by graphene buffer layer in strontium titanate based devices. *J Coll Interf Sci*, 512:767-774. https://doi.org/10.1016/j.jcis.2017.10.113

Wang SY, Tsai CH, Lee DY, et al., 2011. Improved resistive switching properties of Ti/ZrO_2/Pt memory devices for RRAM application. *Microelectron Eng*, 88(7):1628-1632. https://doi.org/10.1016/j.mee.2010.11.058

Wang ZR, Li C, Song WH, et al., 2019. Reinforcement learning with analogue memristor arrays. *Nat Electron*, 2(3):115-124. https://doi.org/10.1038/s41928-019-0221-6

Wu Y, Wei Y, Huang Y, et al., 2017. Capping $CsPbBr_3$ with ZnO to improve performance and stability of perovskite memristors. *Nano Res*, 10(5):1584-1594. https://doi.org/10.1007/s12274-016-1288-2

Xia Y, Zhang C, Wang JX, et al., 2018. Synthesis of transparent aqueous ZrO_2 nanodispersion with a controllable crystalline phase without modification for a high-refractive-index nanocomposite film. *Langmuir*, 34(23): 6806-6813. https://doi.org/10.1021/acs.langmuir.8b00160

Yan XB, Li YC, Zhao JH, et al., 2016. Roles of grain boundary and oxygen vacancies in $Ba_{0.6}Sr_{0.4}TiO_3$ films for resistive switching device application. *Appl Phys Lett*, 108(3): 033108. https://doi.org/10.1063/1.4940198

Yu YM, Yang F, Mao SS, et al., 2018. Effect of anodic oxidation time on resistive switching memory behavior based on amorphous TiO_2 thin films device. *Chem Phys Lett*, 706:477-482. https://doi.org/10.1016/j.cplett.2018.06.063

Zhang YY, Yang T, Yan XB, et al., 2017. A metal/$Ba_{0.6}Sr_{0.4}TiO_3/SiO_2$/Si single film device for charge trapping memory towards a large memory window. *Appl Phys Lett*, 110(22):223501. https://doi.org/10.1063/1.4984220

Zhao H, Dong ZP, Tian H, et al., 2017. Atomically thin femtojoule memristive device. *Adv Mater*, 29(47): 1703232. https://doi.org/10.1002/adma.201703232

Zhou GD, Sun B, Zhou AK, et al., 2017. A larger nonvolatile bipolar resistive switching memory behaviour fabricated using eggshells. *Curr Appl Phys*, 17(2):235-239. https://doi.org/10.1016/j.cap.2016.09.018

Zhou J, Li PG, Zhou YH, et al., 2018. Toward new-generation intelligent manufacturing. *Engineering*, 4(1):11-20. https://doi.org/10.1016/j.eng.2018.01.002

Xiang-lei HE received his BS degree in 2016 from Beijing University of Chemical Technology (BUCT), in Beijing, China,. He is currently a PhD candidate at the State Key Laboratory of Organic-Inorganic Composites of BUCT. His current research focuses on high-gravity-assisted scalable synthesis of functional nanomaterials for high-performance optical devices.

Feng YANG is an associate professor of the Superconductivity and New Energy R&D Center at Southwest Jiaotong University, Chengdu, China. He received his PhD degree in materials science and engineering from Zhejiang University, Hangzhou, China, in 2008. His research interest includes photoelectric nanomaterials, photocatalytic nanomaterials, two-dimensional materials, solar cells, and memristors.

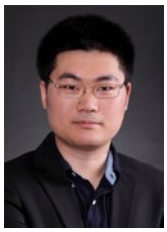

Dan WANG is a professor at the State Key Laboratory of Organic-Inorganic Composites of BUCT in Beijing, China. He received his BS degree in materials science and engineering in 2008 and his PhD degree in optical engineering in 2013, both from Zhejiang University, Hangzhou, China. He was a visiting scholar at Hannam University in the Republic of Korea in 2008-2009, Case Western Reserve University in 2013–2015, and Harvard University in the United States in 2019. His research interest focuses on process intensification in chemical engineering and optical nanomaterials. Dr. Wang serves as an associate editor of *Applied Nanoscience*, an editorial board member of *Transactions of Tianjin University*, a corresponding expert of *Engineering* and *Frontiers of Information Technology & Electronic Engineering*, a youth editorial committee member of *Chinese Journal of Chemical Engineering*, a member of international cooperation committee at Chemical Industry and Engineering Society of China (CIESC), and a senior member of American Institute of Chemical Engineers (AIChE).